Supporting Information

Design and Construction of Porphyrin Box-Based Metal−Organic Frameworks with Hierarchical Superstructures for Efficient Energy Transfer and Photooxidation

Qian Xu,[a, †] Peng Zhang, [a, †] Yuanyuan Sun,[b] Jishi Chen,[a] Chuantao Hou,[a,c,] and Zonghua Wang[a,c,]**

[a] College of Chemistry and Chemical Engineering, Shandong Sino-Japanese Center for Collaborative Research of Carbon Nanomaterials, Instrumental Analysis Center of Qingdao University, Qingdao University, Qingdao 266071, P. R. China

[b] College of Chemistry and Chemical Engineering, Yangzhou University, Yangzhou 225002, P. R. China

[c] Qingdao Application Technology Innovation Center of Photoelectric Biosensing for Clinical Diagnosis and Treatment, Qingdao University, Qingdao 266071, P. R. China

[†] These authors contributed equally to this work.

*Email: houct@qdu.edu.cn; wangzonghua@qdu.edu.cn

S1. Experimental details

S1.1. Chemicals

Meso-tetra(3-carboxyphenyl)porphine (3-TCPP) and 3-TCPP(Zn) were synthesized according to previous reports.[1,2] Zinc chloride ($ZnCl_2$), N,N-dimethylformamide (DMF), tetrahydrofuran (THF), methanol, ethanol, acetone, dichloromethane, acetonitrile, and n-hexane were purchased from Macklin Biochemical Co, Ltd. (Shanghai, China). 1,3-Diphenylisobenzofuran (DPBF), 1,5-dihydroxynaphthalene (DHN-a) and other reagents were purchased from Aladdin Chemistry Company (Shanghai, China). All the reagents are obtained as A. R. purities and without further treatment. 2,6-[4-(tert-butyl)phenyl]-1,5-dihydroxynaphthalene (DHN-b), PCN-222(Zn), and PPF-4(Zn) were synthesized according to the reported literatures.[3-5]

S1.2. Instrumentation

Scanning electron microscopy (SEM) images were obtained using a Hitachi S-8100 field-emission scanning electron microscope. Powder X-ray diffraction (PXRD) patterns were measured using a Bruker D8 ADVANCE diffractometer. Fourier transform-infrared (FT-IR) spectra were recorded on a NICOLET iS50 FT-IR spectrophotometer (Thermo SCIENTIFIC, USA). Thermogravimetry (TG) analysis were performed on a TGA 2050 Thermogravimetric Analyzer at a heating rate of 10 °C/min under an air flow. Ultraviolet−visible (UV−vis) spectra were recorded on a UV-2700 spectrophotometer (Shimadzu, Japan). Fluorescence (PL) emission spectra were measured on a Hitachi F-7000 spectrophotometer (Hitachi, Japan). Supercritical CO_2 drying procedures were performed on a Himatic-250 (Harvent, China) critical point dryer. ^1H nuclear magnetic resonance (NMR) spectrum was measured on a Bruker AVANCE III HD (400 MHz). Liquid chromatograph (LC) curve was recorded on a SPD-M30A.

S1.3. Synthesis of the QPF-2

$ZnCl_2$ (0.079 mmol), 3-TCPP (0.014 mmol), and DMF/EtOH (V/V = 1/1, 5 mL) were mixed and transferred to a 20 mL Teflon autoclave. Then, the mixture was heated in an oven at 140 °C for 72 h. After cooling to room temperature, the purple-red crystals were washed with fresh DMF and collected to obtain QPF-2.

S1.4. Pretreatment and supercritical CO_2 drying of the QPF-2

The QPF-2 was first soaked in fresh DMF to remove unreacted ligands and inorganic species, and was soaked in fresh alcohol to stay for 24 h to exchange and remove the nonvolatile DMF. Then, the QPF-2 was subjected to supercritical CO_2 drying using a Himatic-250 critical point dryer. QPF-2 was placed in the sample chamber and exchanged with liquid CO_2 twice for 2 hours. The chamber temperature was raised to 37 °C, and the chamber pressure was increased to approximately 1200 psi. After maitaining for 2 hours, the supercritical CO_2 was discharged at a very slow rate for 4 h to obtain dry QPF-2.

S1.5. Single-Crystal X-ray Diffraction

The diffraction data of QPF-2 for structure determination were collected with the Bruker D8 Venture Single Crystal X-ray Diffraction using mirror-monochromated Ga-Kα radiation (λ = 1.34139 Å). The data set was corrected by empirical absorption correction using spherical harmonics, implemented in the SADABS scaling algorithm. Due to the massive cell and the large structural voids in QPF-2, the diffraction data was only observed upon to 1.04 Ang resolution. The structure was solved by direct methods and refined by full-matrix least-squares on F^2 with anisotropic displacement by using the SHELXTL software package.[6] Non-hydrogen atoms were refined with anisotropic displacement parameters during the final cycles. Organic hydrogen atoms of ligands were calculated in ideal positions with isotropic displacement parameters set to 1.2 × U_{eq} of the attached atoms. There is large solvent accessible pore volume in the structure of QPF-2, which is occupied by highly disordered DMF molecules. No satisfactory disorder model for these solvent molecules could be achieved, and therefore contributions to scattering due to these solvent molecules were removed using the SQUEEZE routine of PLATON.[7] The details of crystal data and structural refinement can be found in Table S1, Supporting Information, and the provided CIF files.

The diffraction of QPF-2 crystal can be weak because of the large unit cell and disordered solvents. Thus, some alerts are present in the CHECKCIF report. Some common alerts and response are present as follows:

THETM01_ALERT_3_A The value of sine(theta_max)/wavelength is less than 0.550

Calculated sin(theta_max)/wavelength = 0.4792

Response: Due to the massive cell and the large structural voids in QPF-2, the diffraction data was

only observed upon to 1.04 Ang resolution.

PLAT084_ALERT_3_B High wR2 Value (i.e. > 0.25) ..... 0.36 Report

Response: This alert may contribute to the low crystal quality.

PLAT241_ALERT_2_B High 'MainMol' Ueq as Compared to Neighbors of C4 and C5 Check

Response: This alert may contribute to the low crystal quality.

PLAT242_ALERT_2_B Low 'MainMol' Ueq as Compared to Neighbors of Zn6 and C7 Check

Response: This alert may contribute to the low crystal quality.

PLAT420_ALERT_2_B D-H Bond Without Acceptor O9 --H9A . Please Check

PLAT420_ALERT_2_B D-H Bond Without Acceptor O9 --H9B . Please Check

PLAT420_ALERT_2_B D-H Bond Without Acceptor O10 --H10A . Please Check

PLAT420_ALERT_2_B D-H Bond Without Acceptor O10 --H10B . Please Check

PLAT420_ALERT_2_B D-H Bond Without Acceptor O11 --H11A . Please Check

PLAT420_ALERT_2_B D-H Bond Without Acceptor O11 --H11B . Please Check

PLAT420_ALERT_2_B D-H Bond Without Acceptor O13 --H13A . Please Check

PLAT420_ALERT_2_B D-H Bond Without Acceptor O13 --H13B . Please Check

PLAT420_ALERT_2_B D-H Bond Without Acceptor O14 --H14A . Please Check

PLAT420_ALERT_2_B D-H Bond Without Acceptor O14 --H14B . Please Check

Response: The residual electron density map shows that there are large pores in the crystal. Therefore, there is no acceptor for the hydrogen in O9-O14 for the water molecules.

S1.6. Mott-Schottky measurement

Typically, 10 μL of QPF-2 (1 mg mL−1) suspension was dropped onto the surface of the ITO electrode. After drying, the Nafion solution was dropped again to modify the electrode to obtain the working electrode. Mott-Schottky was measured on an electrochemical workstation (CHI 660E) using a standard three-electrode system, with Ag/AgCl as the reference electrode and Pt wire as the counter electrode, and the frequencies were 500, 1000, and 1500 Hz, respectively. A 0.1 M acetonitrile solution of tetrabutylammonium bromide was used as the electrolyte.

S1.7. Detection of singlet oxygen

For the generation of singlet oxygen experiment, acetonitrile solution was bubbled with oxygen for 10 min before measurement, and the experiment was carried out in the presence of oxygen. In a 20

mL oxygen-saturated acetonitrile solution containing 1,3-diphenylisobenzofuran (DPBF) (50 μM) and QPF-2 (40 μg/mL), the absorption spectra of the samples at different reaction times were analyzed using an UV−vis spectrophotometer.

S1.8. Photooxidation of DHN derivatives

Acetonitrile solution was bubbled with oxygen for 10 min before measurement, and the experiment was carried out in the presence of oxygen. QPF-2 (40 μg/mL) was added to the oxygen-saturated acetonitrile solution containing DHN (2×10^{-4} M). Then, a 400 W xenon lamp was irradiated to initiate the reaction. As the reaction proceeded, 0.5 mL of the reaction solution was taken out at specific times, and the UV−vis spectra of these solutions were measured.

S2. Supplementary figures

Table S1. Crystal data and structure refinements for QPF-2.

	QPF-2
Formula	$C_{195}H_{121}N_{17}O_{42}Zn_{12}$
Formula weight	4158.52
Crystal system	orthorhombic
Space group	*F*mmm
a (Å)	29.3869(18)
b	42.172(3)
c (Å)	60.261(4)
α (°)	90
V (Å^3)	74682(8)
Z	8
X-Ray source	Ga-Kα
$d_{calcd.}$ (g/cm^3)	0.740
μ(mm^{-1})	0.766
T (K)	193.00
F(000)	16848.0
θ_{max} [deg]	39.99
Reflns collected	150604
Completeness	99.9%
R_{int}	0.0728
Independent reflns	9112
Data/restraints/para	9112/19/602
GOF on F^2	1.202
R_1, wR_2 [$I > 2\sigma(I)$]	R_1 = 0. 1153, wR_2 = 0. 3348
R_1, wR_2 (all data)	R_1 = 0. 1298, wR_2 = 0. 0.3607
$\Delta\rho_{max}$/ $\Delta\rho_{min}$ [e·Å^{-3}]	1.17/-0.65

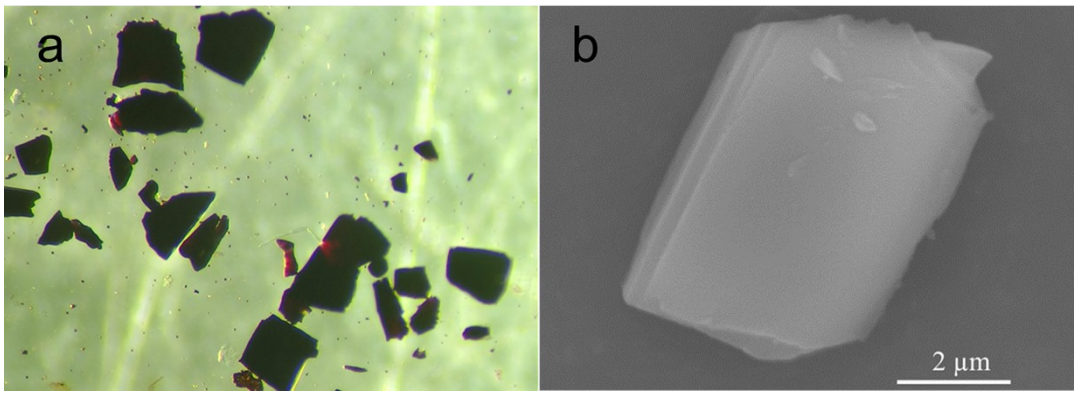

Figure S1. (a) Optical micrograph and (b) SEM image of the QPF-2 crystals.

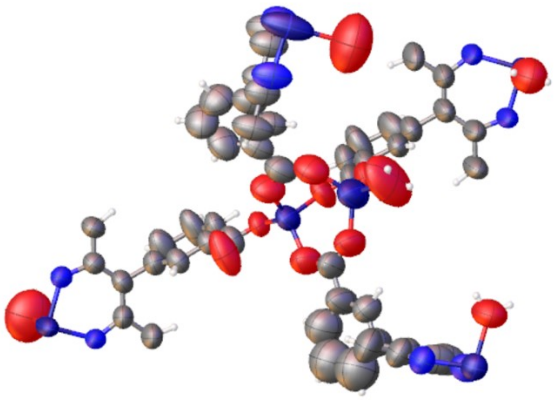

Figure S2. Thermal ellipsoid plot of QPF-2.

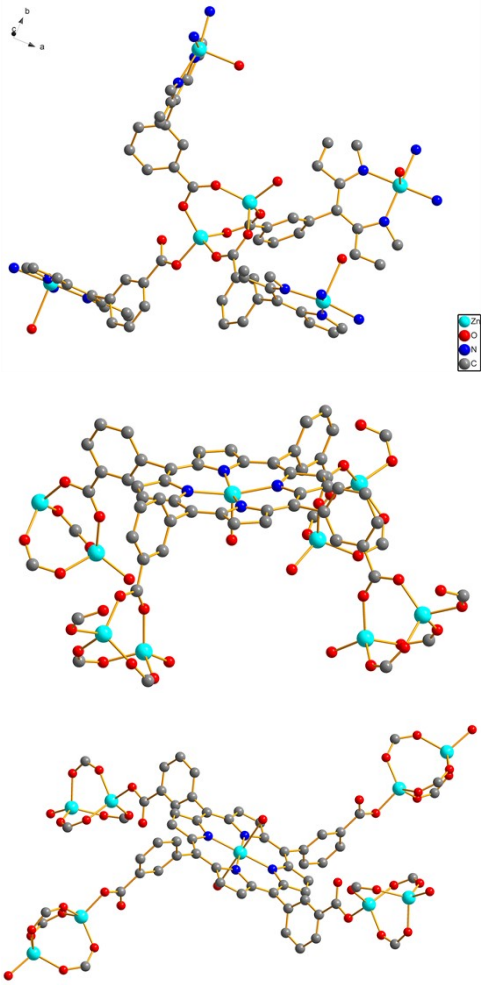

Figure S3. The coordination environment of the Zn_2 node (up). The "table" conformer (middle) and "chair" conformer (down) of 3-TCPP ligand. H atoms are omitted for clarity.

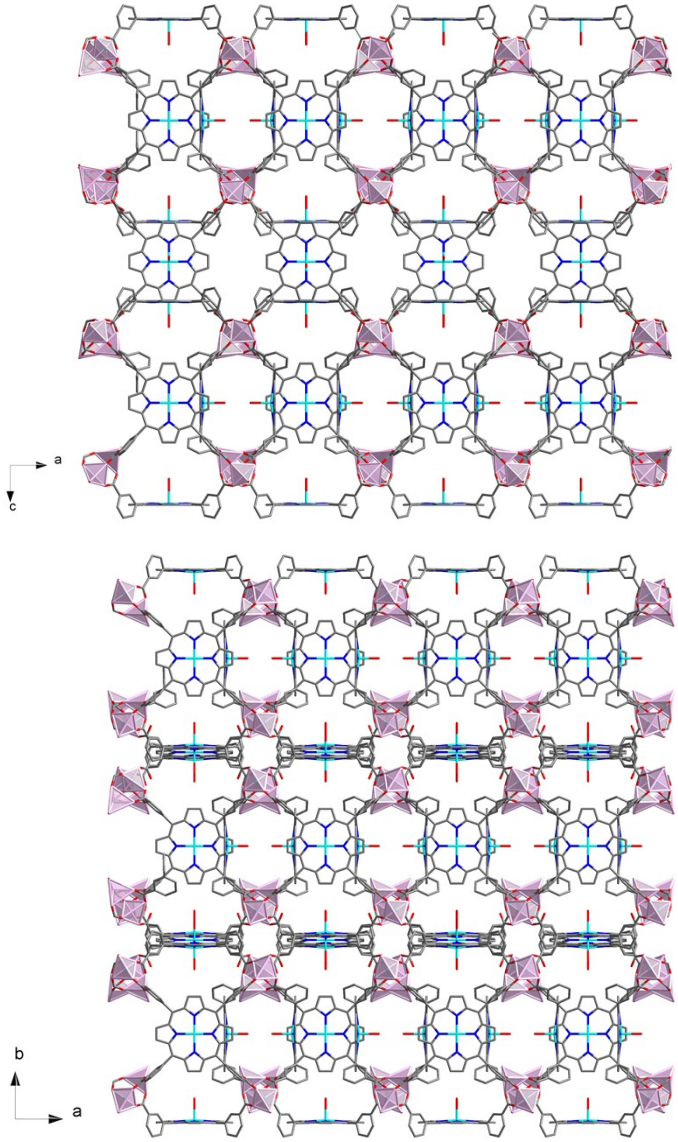

Figure S4. View of the 3D structure of QPF-2 along from the *b*- and *c*-axis. The Zn, O, C, N atoms are shown in cyan, red, gray and blue, respectively. H atoms are omitted for clarity.

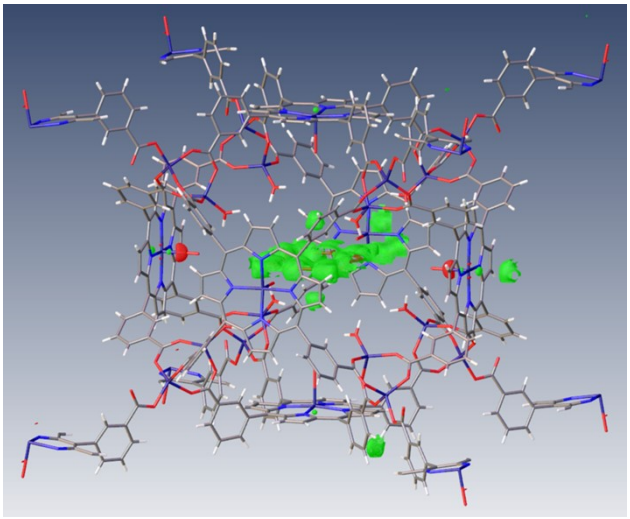

Figure S5. The residual electron density plots (green) in the cavity of QPF-2.

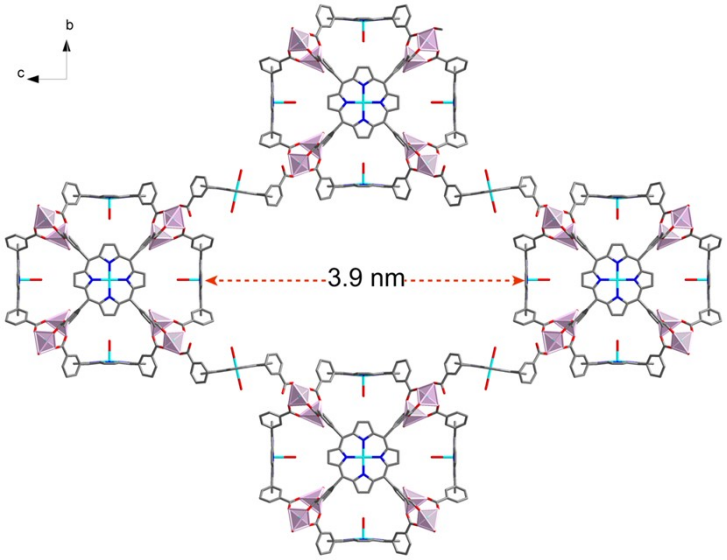

Figure S6. 3-TCPP linkers with "chair" conformer connect and separate adjacent PBs with a distance of 3.9 nm along the *c*-axis.

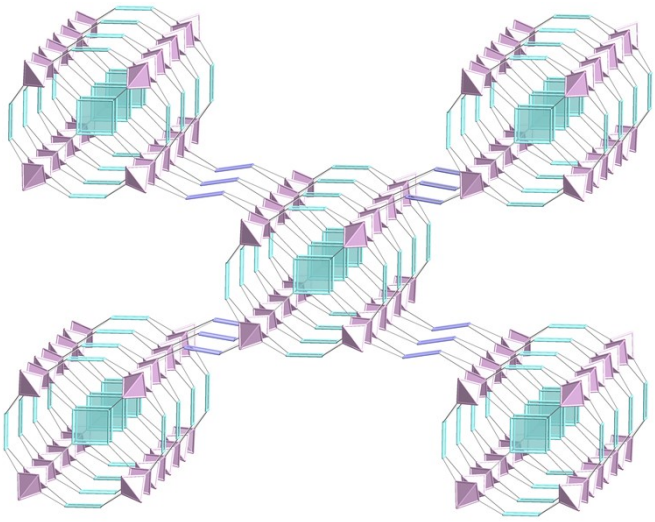

Figure S7. Underlying network topology of one-fold QPF-2.

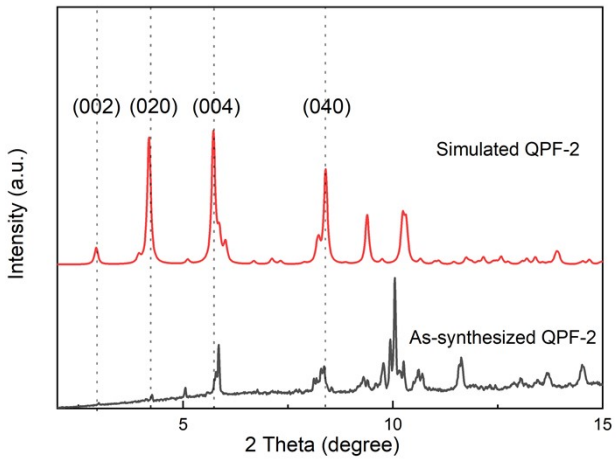

Figure S8. PXRD patterns for the simulated and experimental QPF-2.

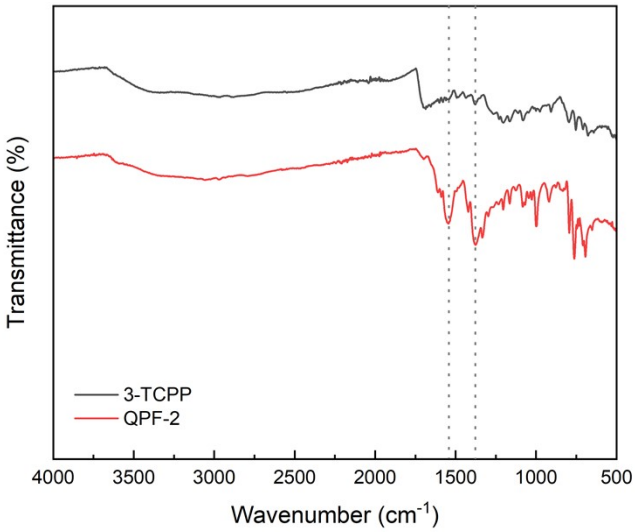

Figure S9. FT-IR spectra for 3-TCPP ligand and the as-synthesized QPF-2.

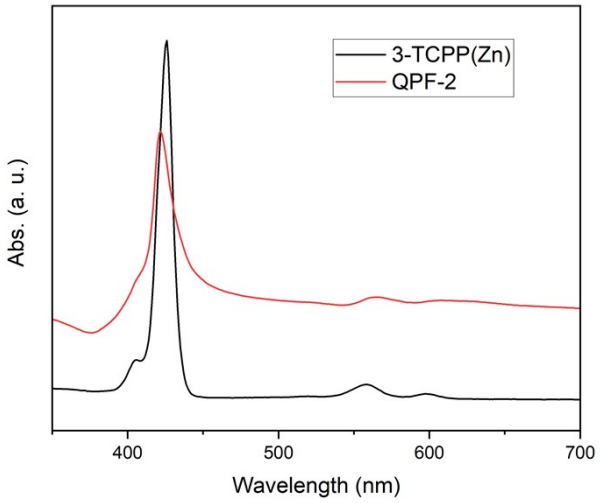

Figure S10. UV−vis spectra for 3-TCPP(Zn) and the as-synthesized QPF-2 in DMF.

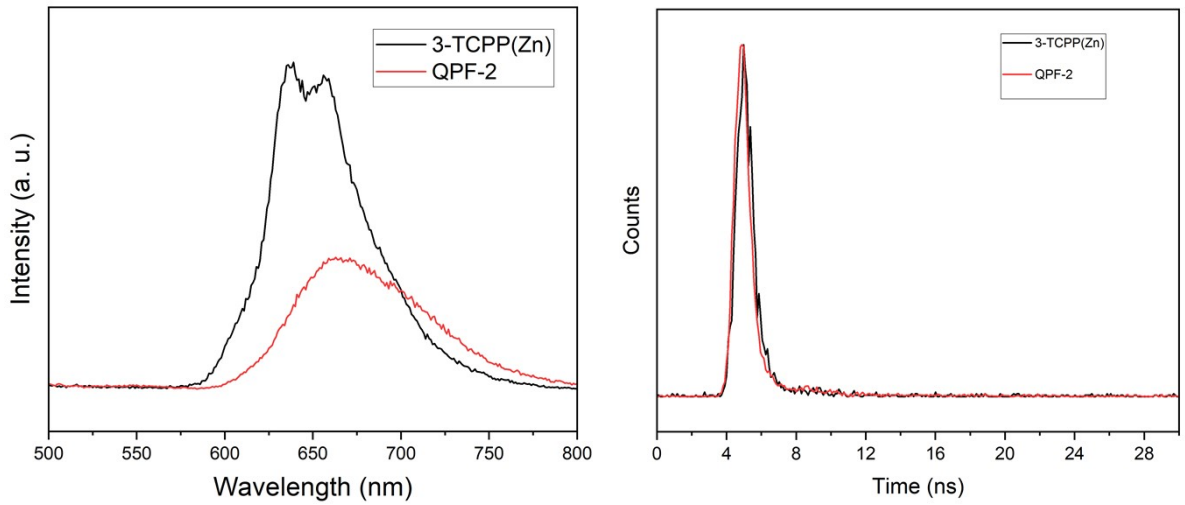

Figure S11. The solid state FL intensity (left) and lifetime (right) of 3-TCPP(Zn) and QPF-2, respectively.

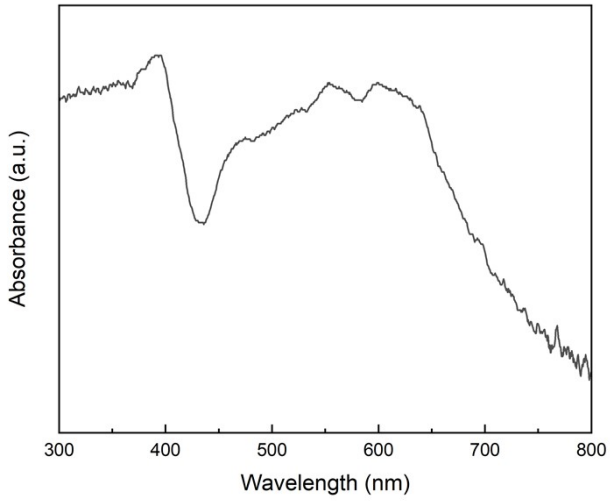

Figure S12. UV−vis DRS of QPF-2.

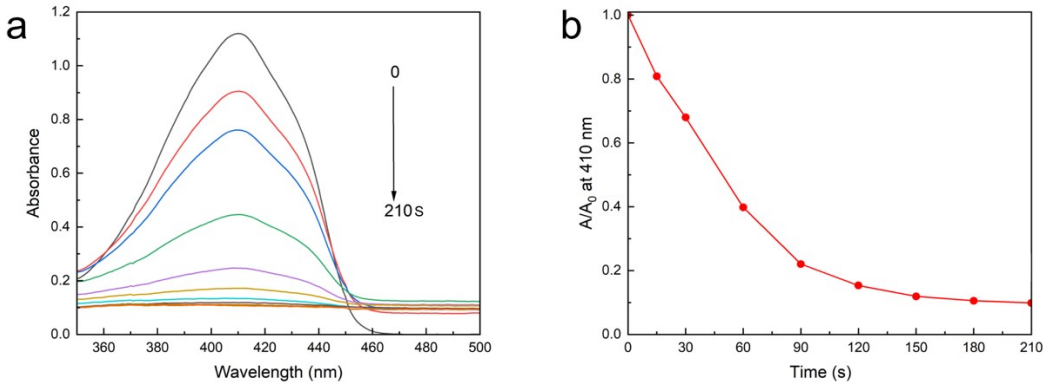

Figure S13. UV−vis absorption spectra (left) and the plots of absorbance decays (right) for DPBF upon visible-light irradiation with QPF-2.

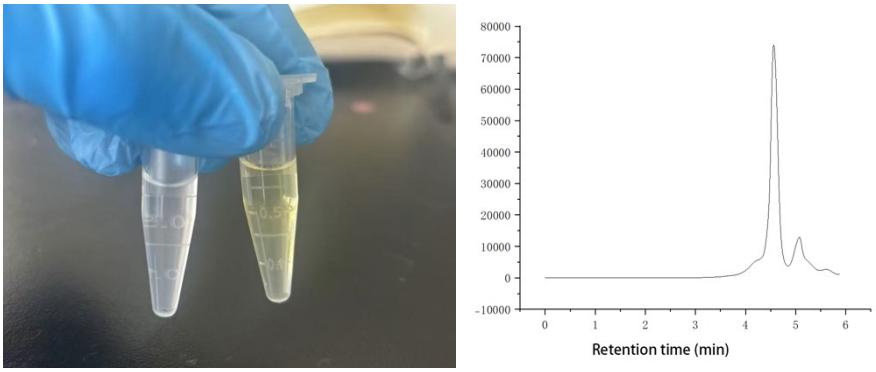

Figure S14. (Left) Photo image of the DHN-a solvent before and after photocatalytic reaction with QPF-2. (Right) liquid chromatography curve of the mixture after photocatalytic reaction.

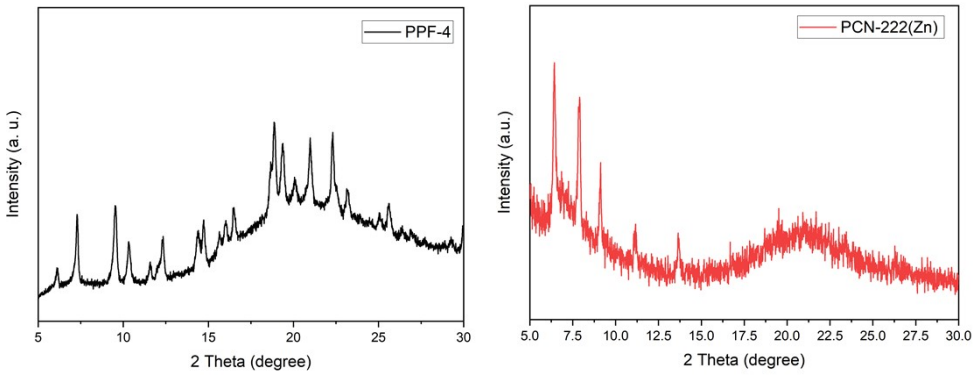

Figure S15. PXRD patterns of experimental PPF-4 and PCN-222(Zn).

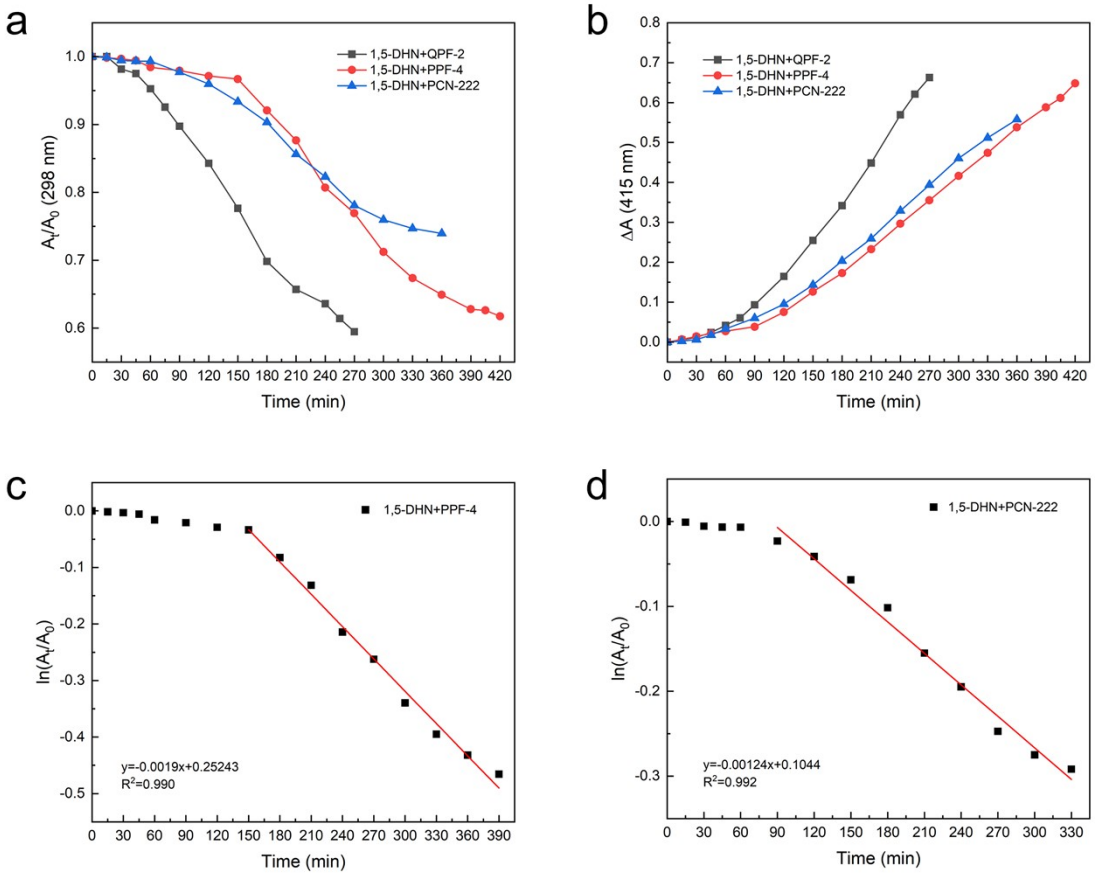

Figure S16. Kinetic study of the photooxidation with MOF catalysts. (a) Plots of A_t/A_0 at 298 nm and (b) absorbance of juglone at 415 nm as a function of reaction time with different catalysts. The conversion rate k_{obs} with (c) PPF-4 and (d) PCN-222(Zn) deduced from $\ln(A_t/A_0)$ versus time.

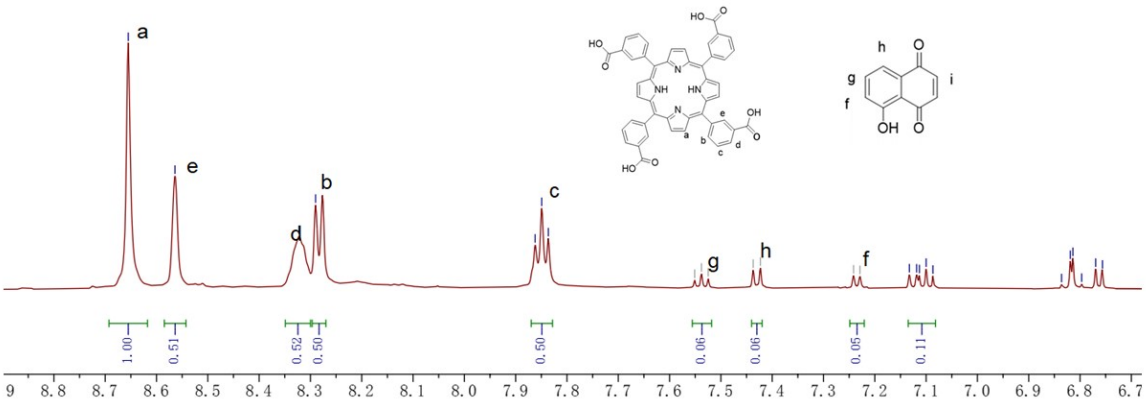

Figure S17. ^{1}H NMR (400 MHz, DMSO-d_6) data of QPF-2 containing juglone after the photocatalytic reaction. δ = (ppm) 8.66 (s, 8H), 8.56 (s, 4H), 8.96 (d, 4H), 8.29 (d, 4H), 7.85 (t, 4H); 7.55 (t, 1H), 7.43 (d, 1H), 7.23 (d, 1H),7.11 (m, 2H).

The sample was treated as follows: after the catalytic reaction was completed, QPF-2 was separated, and the surface attachments were washed with fresh acetonitrile. After drying, QPF-2 was dissolved in D_2SO_4-DMSO-d_6 (1:4) and subjected to ^{1}H NMR mearsurement. The ^{1}H NMR results show that juglone exists in the voids of QPF-2, proving the enhacenment of MOFs pores in the photocatalytic reaction.

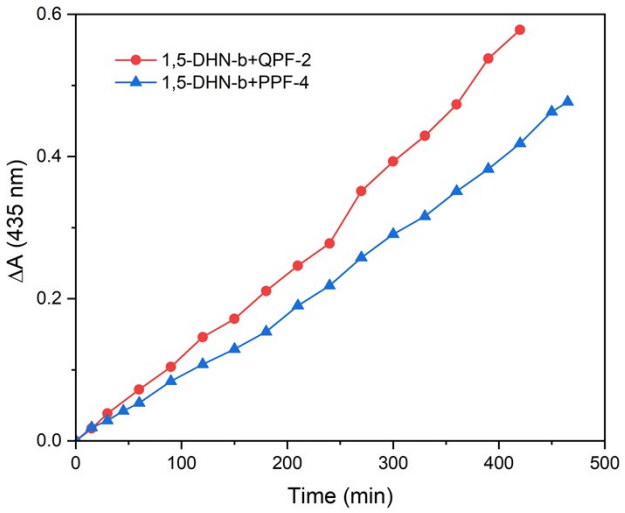

Figure S18. Absorbance at 435 nm as a function of reaction time for the photooxidation of DHN-b with QPF-2 and PPF-4 respectively.

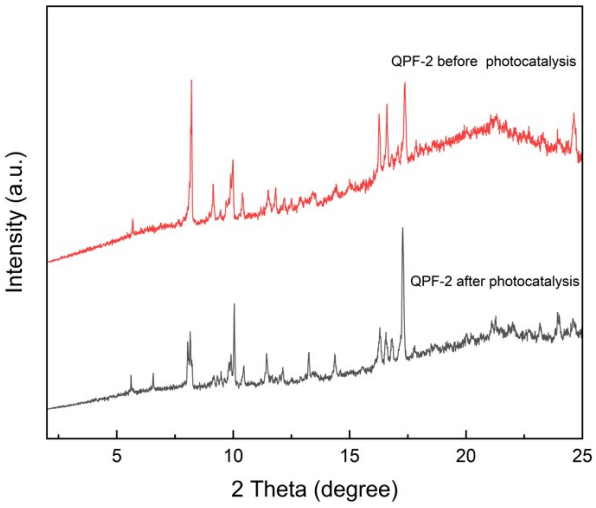

Figure S19. PXRD patterns of the QPF-2 before and after the photocatalytic reactions.

References

1. Eunji Jin, In Seong Lee, Dongwook Kim, Hosoowi Lee, Woo-Dong Jang, Myung Soo Lah, Seung Kyu Min, Wonyoung Choe, *Sci. Adv.* **2019**, 5, eaav4119.

2. Sophia Lipstman and Israel Goldberg, *Cryst. Growth Des.* **2013**, 13, 942−952.

3. Jaehyoung Koo, Ikjin Kim, Younghoon Kim, Dasol Cho, In-Chul Hwang, Rahul Dev Mukhopadhyay, Hayoung Song, Young Ho Ko, Avinash Dhamija, Hochan Lee, Wooseup Hwang, Seungha Kim, Mu-Hyun Baik, Kimoon Kim, *Chem* **2020**, 6, 3374–3384.

4. Dawei Feng, Zhi-Yuan Gu, Jian-Rong Li, Hai-Long Jiang, Zhangwen Wei, Hong-Cai Zhou, *Angew. Chem. Int. Ed.* **2012**, 51, 10307 –10310.

5. Eun-Young Choi, Paul M. Barron, Richard W. Novotny, Hyun-Tak Son, Chunhua Hu, Wonyoung Choe, *Inorg. Chem.* **2009**, 48, 426-428

6. APEX2 v2012.2.0 and SAINT v7.68A data collection and data processing programs, respectively. Bruker Analytical X-ray Instruments, Inc., Madison, WI; SADABS v2008/1 semi-empirical absorption and beam correction program. G.M. Sheldrick, University of Göttingen, Germany.

7. G. M. Sheldrick, SHELXTL, Version 6.14, Structure Determination Software Suite, Bruker AXS, Madison, WI, 2003.